

Observation of $e^+e^- \rightarrow \gamma X(3872)$ at BESIII

M. Ablikim¹, M. N. Achasov^{8,a}, X. C. Ai¹, O. Albayrak⁴, D. J. Ambrose⁴¹, F. F. An¹, Q. An⁴², J. Z. Bai¹, R. Baldini Ferroli^{19A}, Y. Ban²⁸, J. V. Bennett¹⁸, M. Bertani^{19A}, J. M. Bian⁴⁰, E. Boger^{21,b}, O. Bondarenko²², I. Boyko²¹, S. Braun³⁷, R. A. Briere⁴, H. Cai⁴⁷, X. Cai¹, O. Cakir^{36A}, A. Calcaterra^{19A}, G. F. Cao¹, S. A. Cetin^{36B}, J. F. Chang¹, G. Chelkov^{21,b}, G. Chen¹, H. S. Chen¹, J. C. Chen¹, M. L. Chen¹, S. J. Chen²⁶, X. Chen¹, X. R. Chen²³, Y. B. Chen¹, H. P. Cheng¹⁶, X. K. Chu²⁸, Y. P. Chu¹, D. Cronin-Hennessy⁴⁰, H. L. Dai¹, J. P. Dai¹, D. Dedovich²¹, Z. Y. Deng¹, A. Denig²⁰, I. Denysenko²¹, M. Destefanis^{45A,45C}, W. M. Ding³⁰, Y. Ding²⁴, C. Dong²⁷, J. Dong¹, L. Y. Dong¹, M. Y. Dong¹, S. X. Du⁴⁹, J. Z. Fan³⁵, J. Fang¹, S. S. Fang¹, Y. Fang¹, L. Fava^{45B,45C}, C. Q. Feng⁴², C. D. Fu¹, J. L. Fu²⁶, O. Fuks^{21,b}, Q. Gao¹, Y. Gao³⁵, C. Geng⁴², K. Goetzen⁹, W. X. Gong¹, W. Gradl²⁰, M. Greco^{45A,45C}, M. H. Gu¹, Y. T. Gu¹¹, Y. H. Guan¹, A. Q. Guo²⁷, L. B. Guo²⁵, T. Guo²⁵, Y. P. Guo²⁰, Y. L. Han¹, F. A. Harris³⁹, K. L. He¹, M. He¹, Z. Y. He²⁷, T. Held³, Y. K. Heng¹, Z. L. Hou¹, C. Hu²⁵, H. M. Hu¹, J. F. Hu³⁷, T. Hu¹, G. M. Huang⁵, G. S. Huang⁴², J. S. Huang¹⁴, L. Huang¹, X. T. Huang³⁰, Y. Huang²⁶, T. Hussain⁴⁴, C. S. Ji⁴², Q. Ji¹, Q. P. Ji²⁷, X. B. Ji¹, X. L. Ji¹, L. L. Jiang¹, X. S. Jiang¹, J. B. Jiao³⁰, Z. Jiao¹⁶, D. P. Jin¹, S. Jin¹, T. Johansson⁴⁶, N. Kalantar-Nayestanaki²², X. L. Kang¹, X. S. Kang²⁷, M. Kavatsyuk²², B. Kloss²⁰, B. Kopf³, M. Kornicer³⁹, W. Kuehn³⁷, A. Kupsc⁴⁶, W. Lai¹, J. S. Lange³⁷, M. Lara¹⁸, P. Larin¹³, M. Leyhe³, C. H. Li¹, Cheng Li⁴², Cui Li⁴², D. Li¹⁷, D. M. Li⁴⁹, F. Li¹, G. Li¹, H. B. Li¹, J. C. Li¹, K. Li³⁰, K. Li¹², Lei Li¹, P. R. Li³⁸, Q. J. Li¹, T. Li³⁰, W. D. Li¹, W. G. Li¹, X. L. Li³⁰, X. N. Li¹, X. Q. Li²⁷, X. R. Li²⁹, Z. B. Li³⁴, H. Liang⁴², Y. F. Liang³², Y. T. Liang³⁷, D. X. Lin¹³, B. J. Liu¹, C. L. Liu⁴, C. X. Liu¹, F. H. Liu³¹, Fang Liu¹, Feng Liu⁵, H. B. Liu¹¹, H. H. Liu¹⁵, H. M. Liu¹, J. Liu¹, J. P. Liu⁴⁷, K. Liu³⁵, K. Y. Liu²⁴, P. L. Liu³⁰, Q. Liu³⁸, S. B. Liu⁴², X. Liu²³, Y. B. Liu²⁷, Z. A. Liu¹, Zhiqiang Liu¹, Zhiqing Liu²⁰, H. Loehner²², X. C. Lou^{1,c}, G. R. Lu¹⁴, H. J. Lu¹⁶, H. L. Lu¹, J. G. Lu¹, X. R. Lu³⁸, Y. Lu¹, Y. P. Lu¹, C. L. Luo²⁵, M. X. Luo⁴⁸, T. Luo³⁹, X. L. Luo¹, M. Lv¹, F. C. Ma²⁴, H. L. Ma¹, Q. M. Ma¹, S. Ma¹, T. Ma¹, X. Y. Ma¹, F. E. Maas¹³, M. Maggiora^{45A,45C}, Q. A. Malik⁴⁴, Y. J. Mao²⁸, Z. P. Mao¹, J. G. Messchendorp²², J. Min¹, T. J. Min¹, R. E. Mitchell¹⁸, X. H. Mo¹, Y. J. Mo⁵, H. Moeini²², C. Morales Morales¹³, K. Moriya¹⁸, N. Yu. Muchnoi^{8,a}, H. Muramatsu⁴⁰, Y. Nefedov²¹, I. B. Nikolaev^{8,a}, Z. Ning¹, S. Nisar⁷, X. Y. Niu¹, S. L. Olsen²⁹, Q. Ouyang¹, S. Pacetti^{19B}, M. Pelizaeus³, H. P. Peng⁴², K. Peters⁹, J. L. Ping²⁵, R. G. Ping¹, R. Poling⁴⁰, E. Prencipe²⁰, M. Qi²⁶, S. Qian¹, C. F. Qiao³⁸, L. Q. Qin³⁰, X. S. Qin¹, Y. Qin²⁸, Z. H. Qin¹, J. F. Qiu¹, K. H. Rashid⁴⁴, C. F. Redmer²⁰, M. Ripka²⁰, G. Rong¹, X. D. Ruan¹¹, A. Sarantsev^{21,d}, K. Schoenning⁴⁶, S. Schumann²⁰, W. Shan²⁸, M. Shao⁴², C. P. Shen², X. Y. Shen¹, H. Y. Sheng¹, M. R. Shepherd¹⁸, W. M. Song¹, X. Y. Song¹, S. Spataro^{45A,45C}, B. Spruck³⁷, G. X. Sun¹, J. F. Sun¹⁴, S. S. Sun¹, Y. J. Sun⁴², Y. Z. Sun¹, Z. J. Sun¹, Z. T. Sun⁴², C. J. Tang³², X. Tang¹, I. Tapan^{36C}, E. H. Thorndike⁴¹, D. Toth⁴⁰, M. Ullrich³⁷, I. Uman^{36B}, G. S. Varner³⁹, B. Wang²⁷, D. Wang²⁸, D. Y. Wang²⁸, K. Wang¹, L. L. Wang¹, L. S. Wang¹, M. Wang³⁰, P. Wang¹, P. L. Wang¹, Q. J. Wang¹, S. G. Wang²⁸, W. Wang¹, X. F. Wang³⁵, Y. D. Wang^{19A}, Y. F. Wang¹, Y. Q. Wang²⁰, Z. Wang¹, Z. G. Wang¹, Z. H. Wang⁴², Z. Y. Wang¹, D. H. Wei¹⁰, J. B. Wei²⁸, P. Weidenkaff²⁰, S. P. Wen¹, M. Werner³⁷, U. Wiedner³, M. Wolke⁴⁶, L. H. Wu¹, N. Wu¹, Z. Wu¹, L. G. Xia³⁵, Y. Xia¹⁷, D. Xiao¹, Z. J. Xiao²⁵, Y. G. Xie¹, Q. L. Xiu¹, G. F. Xu¹, L. Xu¹, Q. J. Xu¹², Q. N. Xu³⁸, X. P. Xu³³, Z. Xue¹, L. Yan⁴², W. B. Yan⁴², W. C. Yan⁴², Y. H. Yan¹⁷, H. X. Yang¹, Y. Yang⁵, Y. X. Yang¹⁰, H. Ye¹, M. Ye¹, M. H. Ye⁶, B. X. Yu¹, C. X. Yu²⁷, H. W. Yu²⁸, J. S. Yu²³, S. P. Yu³⁰, C. Z. Yuan¹, W. L. Yuan²⁶, Y. Yuan¹, A. A. Zafar⁴⁴, A. Zallo^{19A}, S. L. Zang²⁶, Y. Zeng¹⁷, B. X. Zhang¹, B. Y. Zhang¹, C. Zhang²⁶, C. B. Zhang¹⁷, C. C. Zhang¹, D. H. Zhang¹, H. H. Zhang³⁴, H. Y. Zhang¹, J. J. Zhang¹, J. Q. Zhang¹, J. W. Zhang¹, J. Y. Zhang¹, J. Z. Zhang¹, S. H. Zhang¹, X. J. Zhang¹, X. Y. Zhang³⁰, Y. Zhang¹, Y. H. Zhang¹, Z. H. Zhang⁵, Z. P. Zhang⁴², Z. Y. Zhang⁴⁷, G. Zhao¹, J. W. Zhao¹, Lei Zhao⁴², Ling Zhao¹, M. G. Zhao²⁷, Q. Zhao¹, Q. W. Zhao¹, S. J. Zhao⁴⁹, T. C. Zhao¹, X. H. Zhao²⁶, Y. B. Zhao¹, Z. G. Zhao⁴², A. Zhemchugov^{21,b}, B. Zheng⁴³, J. P. Zheng¹, Y. H. Zheng³⁸, B. Zhong²⁵, L. Zhou¹, Li Zhou²⁷, X. Zhou⁴⁷, X. K. Zhou³⁸, X. R. Zhou⁴², X. Y. Zhou¹, K. Zhu¹, K. J. Zhu¹, X. L. Zhu³⁵, Y. C. Zhu⁴², Y. S. Zhu¹, Z. A. Zhu¹, J. Zhuang¹, B. S. Zou¹, J. H. Zou¹

(BESIII Collaboration)

¹ *Institute of High Energy Physics, Beijing 100049, People's Republic of China*

² *Beihang University, Beijing 100191, People's Republic of China*

³ *Bochum Ruhr-University, D-44780 Bochum, Germany*

⁴ *Carnegie Mellon University, Pittsburgh, Pennsylvania 15213, USA*

⁵ *Central China Normal University, Wuhan 430079, People's Republic of China*

⁶ *China Center of Advanced Science and Technology, Beijing 100190, People's Republic of China*

⁷ *COMSATS Institute of Information Technology, Lahore, Defence Road, Off Raiwind Road, 54000 Lahore*

⁸ *G.I. Budker Institute of Nuclear Physics SB RAS (BINP), Novosibirsk 630090, Russia*

⁹ *GSI Helmholtzcentre for Heavy Ion Research GmbH, D-64291 Darmstadt, Germany*

¹⁰ *Guangxi Normal University, Guilin 541004, People's Republic of China*

- ¹¹ GuangXi University, Nanning 530004, People's Republic of China
- ¹² Hangzhou Normal University, Hangzhou 310036, People's Republic of China
- ¹³ Helmholtz Institute Mainz, Johann-Joachim-Becher-Weg 45, D-55099 Mainz, Germany
- ¹⁴ Henan Normal University, Xixiang 453007, People's Republic of China
- ¹⁵ Henan University of Science and Technology, Luoyang 471003, People's Republic of China
- ¹⁶ Huangshan College, Huangshan 245000, People's Republic of China
- ¹⁷ Hunan University, Changsha 410082, People's Republic of China
- ¹⁸ Indiana University, Bloomington, Indiana 47405, USA
- ¹⁹ (A)INFN Laboratori Nazionali di Frascati, I-00044, Frascati, Italy; (B)INFN and University of Perugia, I-06100, Perugia, Italy
- ²⁰ Johannes Gutenberg University of Mainz, Johann-Joachim-Becher-Weg 45, D-55099 Mainz, Germany
- ²¹ Joint Institute for Nuclear Research, 141980 Dubna, Moscow region, Russia
- ²² KVI, University of Groningen, NL-9747 AA Groningen, The Netherlands
- ²³ Lanzhou University, Lanzhou 730000, People's Republic of China
- ²⁴ Liaoning University, Shenyang 110036, People's Republic of China
- ²⁵ Nanjing Normal University, Nanjing 210023, People's Republic of China
- ²⁶ Nanjing University, Nanjing 210093, People's Republic of China
- ²⁷ Nankai university, Tianjin 300071, People's Republic of China
- ²⁸ Peking University, Beijing 100871, People's Republic of China
- ²⁹ Seoul National University, Seoul, 151-747 Korea
- ³⁰ Shandong University, Jinan 250100, People's Republic of China
- ³¹ Shanxi University, Taiyuan 030006, People's Republic of China
- ³² Sichuan University, Chengdu 610064, People's Republic of China
- ³³ Soochow University, Suzhou 215006, People's Republic of China
- ³⁴ Sun Yat-Sen University, Guangzhou 510275, People's Republic of China
- ³⁵ Tsinghua University, Beijing 100084, People's Republic of China
- ³⁶ (A)Ankara University, Dogol Caddesi, 06100 Tandogan, Ankara, Turkey; (B)Dogus University, 34722 Istanbul, Turkey; (C)Uludag University, 16059 Bursa, Turkey
- ³⁷ Universitaet Giessen, D-35392 Giessen, Germany
- ³⁸ University of Chinese Academy of Sciences, Beijing 100049, People's Republic of China
- ³⁹ University of Hawaii, Honolulu, Hawaii 96822, USA
- ⁴⁰ University of Minnesota, Minneapolis, Minnesota 55455, USA
- ⁴¹ University of Rochester, Rochester, New York 14627, USA
- ⁴² University of Science and Technology of China, Hefei 230026, People's Republic of China
- ⁴³ University of South China, Hengyang 421001, People's Republic of China
- ⁴⁴ University of the Punjab, Lahore-54590, Pakistan
- ⁴⁵ (A)University of Turin, I-10125, Turin, Italy; (B)University of Eastern Piedmont, I-15121, Alessandria, Italy; (C)INFN, I-10125, Turin, Italy
- ⁴⁶ Uppsala University, Box 516, SE-75120 Uppsala
- ⁴⁷ Wuhan University, Wuhan 430072, People's Republic of China
- ⁴⁸ Zhejiang University, Hangzhou 310027, People's Republic of China
- ⁴⁹ Zhengzhou University, Zhengzhou 450001, People's Republic of China
- ^a Also at the Novosibirsk State University, Novosibirsk, 630090, Russia
- ^b Also at the Moscow Institute of Physics and Technology, Moscow 141700, Russia
- ^c Also at University of Texas at Dallas, Richardson, Texas 75083, USA
- ^d Also at the PNPI, Gatchina 188300, Russia

(Dated: March 13, 2018)

With data samples collected with the BESIII detector operating at the BEPCII storage ring at center-of-mass energies from 4.009 to 4.420 GeV, the process $e^+e^- \rightarrow \gamma X(3872)$ is observed for the first time with a statistical significance of 6.3σ . The measured mass of the $X(3872)$ is $(3871.9 \pm 0.7_{\text{stat.}} \pm 0.2_{\text{sys.}}) \text{ MeV}/c^2$, in agreement with previous measurements. Measurements of the product of the cross section $\sigma[e^+e^- \rightarrow \gamma X(3872)]$ and the branching fraction $\mathcal{B}[X(3872) \rightarrow \pi^+\pi^- J/\psi]$ at center-of-mass energies 4.009, 4.229, 4.260, and 4.360 GeV are reported. Our measurements are consistent with expectations for the radiative transition process $Y(4260) \rightarrow \gamma X(3872)$.

The $X(3872)$ was first observed ten years ago by Belle [1] in $B^\pm \rightarrow K^\pm \pi^+ \pi^- J/\psi$ decays; it was subsequently confirmed by several other experiments [2–4]. Since its discovery, the $X(3872)$ has stimulated considerable interest. Both BABAR and Belle observed the $X(3872) \rightarrow \gamma J/\psi$ decay process, which ensures that the $X(3872)$ is a C -even state [5, 6]. The CDF and LHCb experiments determined the spin-parity of the $X(3872)$ to be $J^P = 1^+$ [7, 8], and CDF also found that the $\pi^+ \pi^-$ system was dominated by the $\rho^0(770)$ resonance [9]. Because of the proximity of its mass to the $\bar{D}D^*$ mass threshold, the $X(3872)$ has been interpreted as a candidate for a hadronic molecule or a tetraquark state [10]. Until now, the $X(3872)$ was only observed in B meson decays and hadron collisions. Since the $X(3872)$ is a 1^{++} state, it should be able to be produced through the radiative transition of an excited vector charmonium or charmoniumlike states such as a ψ or a Y .

The puzzling $Y(4260)$ [11] and $Y(4360)$ [12] vector charmoniumlike states have only been observed in final states containing a charmonium meson and a $\pi^+ \pi^-$ pair, in contrast to the $\psi(4040)$ and $\psi(4160)$ which dominantly couple to open charm final states [13]. The observation of the charged charmoniumlike state $Z_c(3900)$ [11, 14], which is clearly not a conventional charmonium state and is produced recoiling against a π^\pm at the CM energy of 4.26 GeV, indicates that these two “exotic” states seem to couple with each other. To better understand their nature, a investigation of other decay processes, such as the radiative transition of the $Y(4260)$ and $Y(4360)$ to lower lying charmonium or charmoniumlike states is important [15]. The process $Y(4260)/Y(4360) \rightarrow \gamma X(3872)$ is unique due to the exotic feature of both the $X(3872)$ and the $Y(4260)$ or $Y(4360)$ resonances.

In this Letter, we report the first observation of the process $e^+e^- \rightarrow \gamma X(3872) \rightarrow \gamma \pi^+ \pi^- J/\psi$, $J/\psi \rightarrow \ell^+ \ell^-$ ($\ell^+ \ell^- = e^+e^-$ or $\mu^+ \mu^-$) in an analysis of data collected with the BESIII detector operating at the BEPCII storage ring [16] at e^+e^- center-of-mass (CM) energies from $\sqrt{s} = 4.009$ GeV to 4.420 GeV [17]. The CM energy is measured with a precision of ± 1.0 MeV [18]. A GEANT4-based Monte Carlo (MC) simulation software package that includes the geometric description of the BESIII detector and the detector response is used to optimize the event selection criteria, determine the detection efficiency, and estimate backgrounds. For the signal process, we generate $e^+e^- \rightarrow \gamma X(3872)$, with $X(3872) \rightarrow \pi^+ \pi^- J/\psi$ at each CM energy. Initial state radiation (ISR) is simulated with KKMC [19], where the Born cross section of $e^+e^- \rightarrow \gamma X(3872)$ between 3.90 and 4.42 GeV is assumed to follow the $e^+e^- \rightarrow \pi^+ \pi^- J/\psi$ line-shape [11]. The maximum ISR photon energy corresponds to the 3.9 GeV/ c^2 production threshold of the $\gamma X(3872)$ system. We generate $X(3872) \rightarrow \rho^0 J/\psi$ MC events with $\rho^0 \rightarrow \pi^+ \pi^-$ to model the $\pi^+ \pi^-$ system and determine the detection efficiency [9]. Here the ρ^0 and J/ψ are assumed to be in a relative S -wave. Final State Radiation (FSR) is handled with PHOTOS [20].

Events with four good charged tracks with net charge zero are selected as described in Ref. [14]. Showers identified as photon candidates must satisfy fiducial and shower quality as well as timing requirement as described in Ref. [21]. When there is more than one photon candidate, the one with the largest energy is regarded as the radiative photon. In order to improve the momentum and energy resolution and reduce the background, the event is subjected to a four-constraint (4C) kinematic fit to the hypothesis $e^+e^- \rightarrow \gamma \pi^+ \pi^- \ell^+ \ell^-$, that constrains total four momentum of the measured particles to be equal to the initial four-momentum of the colliding beams. The χ^2 of the kinematic fit is required to be less than 60. To reject radiative Bhabha and radiative dimuon ($\gamma e^+e^-/\gamma \mu^+ \mu^-$) backgrounds associated with photon-conversion, the cosine of the opening angle of the pion candidates, is required to be less than 0.98. This restriction removes almost all the background events with an efficiency loss for signal that is less than 1%. Background from $e^+e^- \rightarrow \eta J/\psi$ with $\eta \rightarrow \gamma \pi^+ \pi^-/\pi^+ \pi^- \pi^0$ is rejected by requiring $M(\gamma \pi^+ \pi^-) > 0.6$ GeV/ c^2 , and its remaining contribution is negligible [21, 22].

After imposing the above requirements, there are clear J/ψ peaks in the $\ell^+ \ell^-$ invariant mass distribution at each CM energy data set. The J/ψ mass window to select signal events is $3.08 < M(\ell^+ \ell^-) < 3.12$ GeV/ c^2 (mass resolution is 6 MeV/ c^2), while the sidebands are $3.0 < M(\ell^+ \ell^-) < 3.06$ GeV/ c^2 and $3.14 < M(\ell^+ \ell^-) < 3.20$ GeV/ c^2 , which is three times as wide as the signal region.

The remaining backgrounds mainly come from $e^+e^- \rightarrow (\gamma_{\text{ISR}}) \pi^+ \pi^- J/\psi$, $\eta' J/\psi$, and $\pi^+ \pi^- \pi^+ \pi^- \pi^0/\pi^+ \pi^- \pi^+ \pi^- \gamma$. MC simulation based on available measurements for $(\gamma_{\text{ISR}}) \pi^+ \pi^- J/\psi$ [11], and cross sections measured from the same data samples for $\eta' J/\psi$ ($\eta' \rightarrow \gamma \pi^+ \pi^-/\pi^+ \pi^- \eta$) shows a smooth, non-peaking $M(\pi^+ \pi^- J/\psi)$ mass distribution in the $X(3872)$ signal region, and indicates that background from $e^+e^- \rightarrow \pi^+ \pi^- \pi^+ \pi^- (\pi^0/\gamma)$ is small and can be estimated from the J/ψ mass sideband data. Figure 1 shows the $\pi^+ \pi^- J/\psi$ invariant mass distributions at $\sqrt{s} = 4.009, 4.229, 4.260,$ and 4.360 GeV. Here $M(\pi^+ \pi^- J/\psi) = M(\pi^+ \pi^- \ell^+ \ell^-) - M(\ell^+ \ell^-) + m(J/\psi)$ is used to reduce the resolution effect of the lepton pairs, and $m(J/\psi)$ is the nominal mass of J/ψ [13]. There is a huge $e^+e^- \rightarrow \gamma_{\text{ISR}} \psi(3686)$ signal at each CM energy data set. In addition, there is a narrow peak around 3872 MeV/ c^2 in the 4.229 and 4.260 GeV data samples, while there is no significant signal at the other energies.

The $M(\pi^+ \pi^- J/\psi)$ distribution (summed over all CM energy data sets) is fitted to determine the mass and $X(3872)$ yield. We use a MC simulated signal histogram convolved with a Gaussian function which represents the resolution difference between data and MC simulation as the signal shape, and a linear function for the background. The ISR $\psi(3686)$ signal is used to calibrate the absolute mass scale and to extract the resolution difference between data and MC sim-

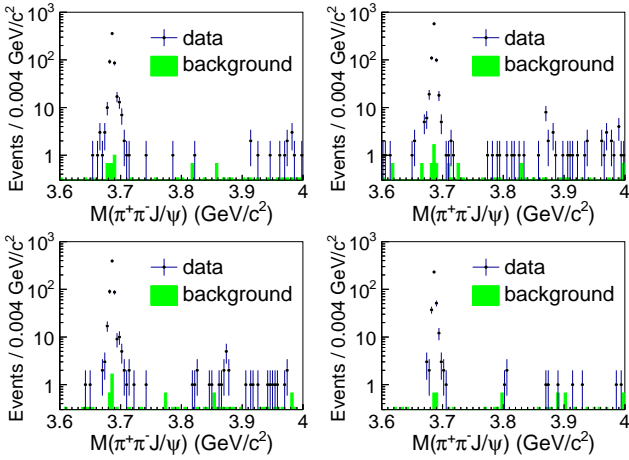


FIG. 1: The $\pi^+\pi^-J/\psi$ invariant mass distributions at $\sqrt{s} = 4.009$ (top left), 4.229 (top right), 4.260 (bottom left), and 4.360 GeV (bottom right). Dots with error bars are data, the green shaded histograms are normalized J/ψ sideband events.

ulation. The fit to the $\psi(3686)$ results in a mass shift of $\mu_{\psi(3686)} = -(0.34 \pm 0.04) \text{ MeV}/c^2$, and a standard deviation of the Gaussian resolution function of $\sigma = (1.14 \pm 0.07) \text{ MeV}/c^2$. The resolution parameter of the resolution Gaussian applied to the MC simulated signal shape is fixed at $1.14 \text{ MeV}/c^2$ in the fit to the $X(3872)$. Figure 2 shows the fit result (with $M[X(3872)]_{\text{input}} = 3871.7 \text{ MeV}/c^2$ as input in MC simulation), which gives $\mu_{X(3872)} = -(0.10 \pm 0.69) \text{ MeV}/c^2$ and $N[X(3872)] = 20.1 \pm 4.5$. So, the measured mass of $X(3872)$ is $M[X(3872)] = M[X(3872)]_{\text{input}} + \mu_{X(3872)} - \mu_{\psi(3686)} = (3871.9 \pm 0.7) \text{ MeV}/c^2$, where the uncertainty includes the statistical uncertainties from the fit and the mass calibration. The limited statistics prevent us from measuring the intrinsic width of the $X(3872)$. From a fit with a floating width we obtain $\Gamma[X(3872)] = (0.0^{+1.7}_{-0.0}) \text{ MeV}$, or less than 2.4 MeV at the 90% confidence level (C.L.). The statistical significance of $X(3872)$ is 6.3σ , estimated by comparing the difference of log-likelihood value [$\Delta(-2 \ln \mathcal{L}) = 44.5$] with and without the $X(3872)$ signal in the fit, and taking the change of the number-of-degrees-of-freedom ($\Delta\text{ndf}=2$) into consideration.

Figure 3 shows the angular distribution of the radiative photon in the e^+e^- CM frame and the $\pi^+\pi^-$ invariant mass distribution, for the $X(3872)$ signal events ($3.86 < M(\pi^+\pi^-J/\psi) < 3.88 \text{ GeV}/c^2$) and normalized sideband events ($3.83 < M(\pi^+\pi^-J/\psi) < 3.86 \text{ GeV}/c^2$ or $3.88 < M(\pi^+\pi^-J/\psi) < 3.91 \text{ GeV}/c^2$). The data agree with MC simulation assuming a pure $E1$ -transition between the $Y(4260)$ and the $X(3872)$ for the polar angle distribution, and the $M(\pi^+\pi^-)$ distribution is consistent with the CDF observation [9] of a dominant $\rho^0(770)$ resonance contribution.

The product of the Born-order cross section times the branching fraction of $X(3872) \rightarrow \pi^+\pi^-J/\psi$ is calculated using $\sigma^B[e^+e^- \rightarrow \gamma X(3872)] \times \mathcal{B}[X(3872) \rightarrow \pi^+\pi^-J/\psi] = \frac{N^{\text{obs}}}{\mathcal{L}_{\text{int}}(1+\delta)\epsilon\mathcal{B}}$, where N^{obs} is the number of observed events ob-

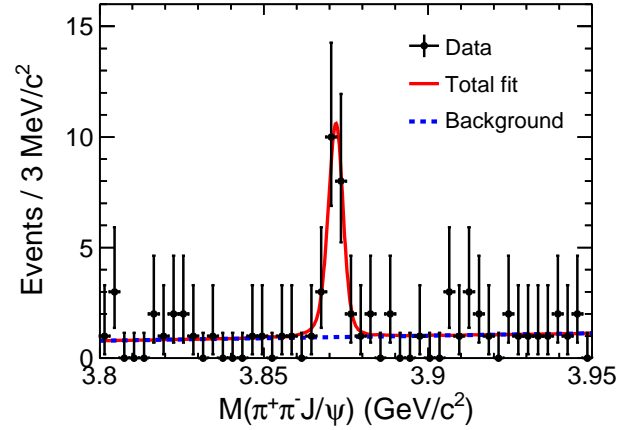


FIG. 2: Fit of the $M(\pi^+\pi^-J/\psi)$ distribution with a MC simulated histogram convolved with a Gaussian function for signal and a linear background function. Dots with error bars are data, the red curve shows the total fit result, while the blue dashed curve shows the background contribution.

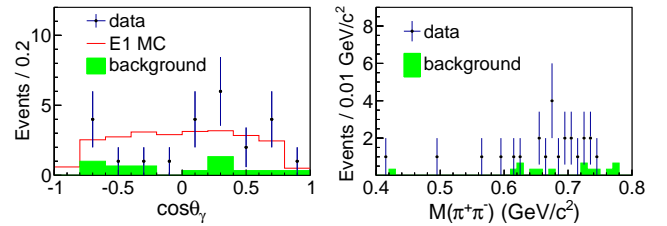


FIG. 3: The $\cos \theta$ distribution of the radiative photon in e^+e^- CM frame (left) and the $M(\pi^+\pi^-)$ distribution (right). Dots with error bars are data in the $X(3872)$ signal region, the green shaded histograms are normalized $X(3872)$ sideband events, and the red open histogram in the left panel is the result from a MC simulation that assumes a pure $E1$ -transition.

tained from the fit to the $M(\pi^+\pi^-J/\psi)$ distribution, \mathcal{L}_{int} is integrated luminosity, ϵ is the detection efficiency, \mathcal{B} is the branching fraction of $J/\psi \rightarrow \ell^+\ell^-$ and $(1+\delta)$ is the radiative correction factor, which depends on the line shape of $e^+e^- \rightarrow \gamma X(3872)$. Since we observe large cross sections at $\sqrt{s} = 4.229$ and 4.260 GeV , we assume the $e^+e^- \rightarrow \gamma X(3872)$ cross section follows that of $e^+e^- \rightarrow \pi^+\pi^-J/\psi$ over the full energy range of interest and use the $e^+e^- \rightarrow \pi^+\pi^-J/\psi$ line-shape from published results [11] as input in the calculation of the efficiency and radiative correction factor. The results of these studies at different energies ($\sqrt{s} = 4.009 \text{ GeV}$, 4.229 GeV , 4.260 GeV , and 4.360 GeV) are listed in Table I. For the 4.009 GeV and 4.360 GeV data, where the $X(3872)$ signal is not statistically significant, upper limits for production yield at 90% C.L. are also given. As a validation, the measured ISR $\psi(3686)$ cross section at each energy, together with the corresponding QED prediction [23] are also listed in Table I, where there is good agreement.

We fit the energy-dependent cross section with a $Y(4260)$

TABLE I: The number of $X(3872)$ events (N^{obs}), radiative correction factor ($1 + \delta$), detection efficiency (ϵ), measured Born cross section $\sigma^B[e^+e^- \rightarrow \gamma X(3872)]$ times $\mathcal{B}[X(3872) \rightarrow \pi^+\pi^- J/\psi]$ ($\sigma^B \cdot \mathcal{B}$, where the first uncertainties are statistical and the second systematic), measured ISR $\psi(3686)$ cross section (σ^{ISR} , where the first uncertainties are statistical and the second systematic), and predicted ISR $\psi(3686)$ cross section (σ^{QED} with uncertainties from resonant parameters) from QED [23] using resonant parameters in PDG [13] as input at different energies. For 4.009 GeV and 4.360 GeV, the upper limits of observed events (N^{up}) and cross section times branching fraction ($\sigma^{\text{up}} \cdot \mathcal{B}$) are given at the 90% C.L.

\sqrt{s} (GeV)	N^{obs}	N^{up}	ϵ (%)	$1 + \delta$	$\sigma^B \cdot \mathcal{B}$ (pb)	$\sigma^{\text{up}} \cdot \mathcal{B}$ (pb)	σ^{ISR} (pb)	σ^{QED} (pb)
4.009	0.0 ± 0.5	< 1.4	28.7	0.861	$0.00 \pm 0.04 \pm 0.01$	< 0.11	$719 \pm 30 \pm 47$	735 ± 13
4.229	9.6 ± 3.1	-	34.4	0.799	$0.27 \pm 0.09 \pm 0.02$	-	$404 \pm 14 \pm 27$	408 ± 7
4.260	8.7 ± 3.0	-	33.1	0.814	$0.33 \pm 0.12 \pm 0.02$	-	$378 \pm 16 \pm 25$	382 ± 7
4.360	1.7 ± 1.4	< 5.1	23.2	1.023	$0.11 \pm 0.09 \pm 0.01$	< 0.36	$308 \pm 17 \pm 20$	316 ± 5

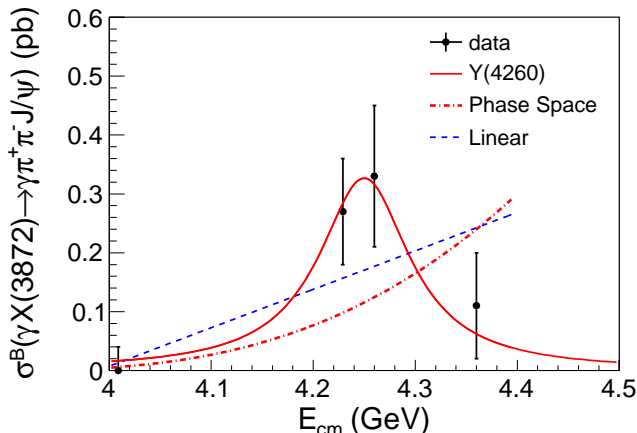


FIG. 4: The fit to $\sigma^B[e^+e^- \rightarrow \gamma X(3872)] \times \mathcal{B}[X(3872) \rightarrow \pi^+\pi^- J/\psi]$ with a $Y(4260)$ resonance (red solid curve), a linear continuum (blue dashed curve), or a $E1$ -transition phase space ($\propto E_\gamma^3$) term (red dotted-dashed curve). Dots with error bars are data.

resonance (parameters fixed to PDG [13] values), a linear continuum, or a $E1$ -transition phase space ($\propto E_\gamma^3$) term. Figure 4 shows all the fit results, which give $\chi^2/\text{ndf} = 0.49/3$ (C.L.=92%), $5.5/2$ (C.L.=6%), and $8.7/3$ (C.L.=3%) for a $Y(4260)$ resonance, linear continuum, and phase space distribution, respectively. The $Y(4260)$ resonance describes the data better than the other two options.

The systematic uncertainty in the $X(3872)$ mass measurement include those from the absolute mass scale and the parametrization of the $X(3872)$ signal and background shapes. Since we use ISR $\psi(3686)$ events to calibrate the fit, the systematic uncertainty from the mass scale is estimated to be $0.1 \text{ MeV}/c^2$ (including statistical uncertainties of the MC samples used in calibration procedure). In the $X(3872)$ mass fit, a MC simulated histogram with a zero width is used to parameterize the signal shape. We replace this histogram with a simulated $X(3872)$ resonance with a width of 1.2 MeV [13] (the upper limit of the $X(3872)$ width at 90% C.L.) and repeat the fit; the change in mass for this new fit is taken as the systematic uncertainty due to the signal parametrization,

which is $0.1 \text{ MeV}/c^2$. Likewise, changes measured with a background shape from MC-simulated ($\gamma_{\text{ISR}}\pi^+\pi^- J/\psi$ and $\eta' J/\psi$ events indicate a systematic uncertainty associated with the background shape of $0.1 \text{ MeV}/c^2$ in mass. By summing the contributions from all sources assuming that they are independent, we obtain a total systematic uncertainty of $0.2 \text{ MeV}/c^2$ for the $X(3872)$ mass measurement.

The systematic uncertainty in the cross section measurement mainly comes from efficiencies, signal parametrization, background shape, radiative correction, and luminosity measurement. The luminosity is measured using Bhabha events, with an uncertainty of 1.0%. The uncertainty of tracking efficiency for high momenta leptons is 1.0% per track. Pions have momentum ranges from 0.1 to $0.6 \text{ GeV}/c$ at $\sqrt{s} = 4.260 \text{ GeV}$, and with a small change with different CM energies. The momentum-weighted uncertainty is also estimated to be 1.0% per track. In this analysis, the radiative photons have energies that several hundreds of MeV. Studies with a sample of $J/\psi \rightarrow \rho\pi$ events show that the uncertainty in the reconstruction efficiency for photons in this energy range is less than 1.0%.

The number of $X(3872)$ signal events is obtained through a fit to the $M(\pi^+\pi^- J/\psi)$ distribution. In the nominal fit, a simulated histogram with zero width convolved with a Gaussian function is used to parameterize the $X(3872)$ signal. When a MC-simulated signal shape with $\Gamma[X(3872)] = 1.2 \text{ MeV}$ [13] is used, the difference in the $X(3872)$ signal yield, is 4.0%; this is taken as the systematic uncertainty due to signal parametrization. Changing the background shape from a linear term to the expected shape from the dominant background source $\eta' J/\psi$ results in a 0.2% difference in the $X(3872)$ yields. The $e^+e^- \rightarrow \pi^+\pi^- J/\psi$ line shape affects the radiative correction factor and detection efficiency. Using the measurements from BESIII, Belle, and BABAR [11] as inputs, the maximum difference in $(1 + \delta)\epsilon$ is 0.6%, which is taken as the systematic uncertainty. The uncertainty from the kinematic fit is estimated with the very pure ISR $\psi(3686)$ sample, and the efficiency difference between data and MC simulation is found to be 1.5%. The systematic uncertainty for the J/ψ mass window is also estimated using the ISR $\psi(3686)$ events, and the efficiency difference between data and MC simulation is found to be $(0.8 \pm 0.8)\%$. We conservatively take 1.6% as the systematic uncertainty due to J/ψ mass window. The un-

certainty in the branching fraction of $J/\psi \rightarrow \ell^+\ell^-$ is taken from Ref. [13]. The efficiencies for other selection criteria, the trigger simulation, the event start time determination, and the final-state-radiation simulation are quite high ($> 99\%$), and their systematic uncertainties are estimated to be less than 1%. Assuming all the systematic uncertainty sources are independent, we add all of them in quadrature, and the total systematic uncertainty is estimated to be 6.5%.

In summary, we report the first observation of the process $e^+e^- \rightarrow \gamma X(3872)$. The measured mass of the $X(3872)$, $M[X(3872)] = (3871.9 \pm 0.7 \pm 0.2) \text{ MeV}/c^2$, agrees well with previous measurements [13]. The production rate $\sigma^B[e^+e^- \rightarrow \gamma X(3872)] \cdot \mathcal{B}[X(3872) \rightarrow \pi^+\pi^- J/\psi]$ is measured to be $(0.27 \pm 0.09 \pm 0.02) \text{ pb}$ at $\sqrt{s} = 4.229 \text{ GeV}$, $(0.33 \pm 0.12 \pm 0.02) \text{ pb}$ at $\sqrt{s} = 4.260 \text{ GeV}$, less than 0.11 pb at $\sqrt{s} = 4.009 \text{ GeV}$, and less than 0.36 pb at $\sqrt{s} = 4.360 \text{ GeV}$ at the 90% C.L. Here the first uncertainties are statistical and the second systematic. (For the upper limits, the efficiency has been lowered by a factor of $(1 - \sigma_{\text{sys}})$.)

These observations strongly support the existence of the radiative transition process $Y(4260) \rightarrow \gamma X(3872)$. While the measured cross sections at around 4.260 GeV are an order of magnitude higher than the NRQCD calculation of continuum production [24], the resonant contribution with $Y(4260)$ line shape provides a better description of the data than either a linear continuum or a $E1$ -transition phase space distribution. The $Y(4260) \rightarrow \gamma X(3872)$ could be another previously unseen decay mode of the $Y(4260)$ resonance. This, together with the previously reported transitions to the charged charmoniumlike state $Z_c(3900)$ (which is manifestly exotic) [11, 14], suggest that there might be some commonality in the nature of these three different states. This may be a clue that can facilitate a better theoretical interpretation of them. As an example, the measured relative large $\gamma X(3872)$ production rate near 4.260 GeV is similar to the model dependent calculations in Ref. [15] where the $Y(4260)$ is taken as a

$\bar{D}D_1$ molecule.

Combining with the $e^+e^- \rightarrow \pi^+\pi^- J/\psi$ cross section measurement at $\sqrt{s} = 4.260 \text{ GeV}$ from BESIII [14], we obtain $\sigma^B[e^+e^- \rightarrow \gamma X(3872)] \cdot \mathcal{B}[X(3872) \rightarrow \pi^+\pi^- J/\psi] / \sigma^B(e^+e^- \rightarrow \pi^+\pi^- J/\psi) = (5.2 \pm 1.9) \times 10^{-3}$, under the assumption that the $X(3872)$ is produced only from the $Y(4260)$ radiative decays and the $\pi^+\pi^- J/\psi$ is only from the $Y(4260)$ hadronic decays. If we take $\mathcal{B}[X(3872) \rightarrow \pi^+\pi^- J/\psi] = 5\%$ [25], then $\mathcal{R} = \frac{\sigma^B[e^+e^- \rightarrow \gamma X(3872)]}{\sigma^B(e^+e^- \rightarrow \pi^+\pi^- J/\psi)} = 0.1$, or equivalently, $\frac{\mathcal{B}[Y(4260) \rightarrow \gamma X(3872)]}{\mathcal{B}[Y(4260) \rightarrow \pi^+\pi^- J/\psi]} = 0.1$.

The BESIII collaboration thanks the staff of BEPCII and the computing center for their strong support. This work is supported in part by the Ministry of Science and Technology of China under Contract No. 2009CB825200; National Natural Science Foundation of China (NSFC) under Contracts Nos. 10625524, 10821063, 10825524, 10835001, 10935007, 11125525, 11235011; Joint Funds of the National Natural Science Foundation of China under Contracts Nos. 11079008, 11179007; the Chinese Academy of Sciences (CAS) Large-Scale Scientific Facility Program; CAS under Contracts Nos. KJCX2-YW-N29, KJCX2-YW-N45; 100 Talents Program of CAS; German Research Foundation DFG under Contract No. Collaborative Research Center CRC-1044; Seventh Framework Programme of the European Union under Marie Curie International Incoming Fellowship Grant Agreement No. 627240; Istituto Nazionale di Fisica Nucleare, Italy; Ministry of Development of Turkey under Contract No. DPT2006K-120470; U. S. Department of Energy under Contracts Nos. DE-FG02-04ER41291, DE-FG02-05ER41374, DE-FG02-94ER40823, DESC0010118; U.S. National Science Foundation; University of Groningen (RuG) and the Helmholtzzentrum fuer Schwerionenforschung GmbH (GSI), Darmstadt; WCU Program of National Research Foundation of Korea under Contract No. R32-2008-000-10155-0.

-
- [1] S. K. Choi *et al.* (Belle Collaboration), *Phys. Rev. Lett.* **91**, 262001 (2003).
- [2] D. Acosta *et al.* (CDF Collaboration), *Phys. Rev. Lett.* **93**, 072001 (2004).
- [3] V. M. Abazov *et al.* (D0 Collaboration), *Phys. Rev. Lett.* **93**, 162002 (2004).
- [4] B. Aubert *et al.* (BABAR Collaboration), *Phys. Rev. D* **71**, 071103 (2005).
- [5] B. Aubert *et al.* (BABAR Collaboration), *Phys. Rev. D* **74**, 071101 (2006).
- [6] V. Bhardwaj *et al.* (Belle Collaboration), *Phys. Rev. Lett.* **107**, 091803 (2011).
- [7] A. Abulencia *et al.* (CDF Collaboration), *Phys. Rev. Lett.* **98**, 132002 (2007).
- [8] R. Aaij *et al.* (LHCb Collaboration), *Eur. Phys. J. C* **72**, 1972 (2012); arXiv:1302.6269.
- [9] A. Abulencia *et al.* (CDF Collaboration), *Phys. Rev. Lett.* **96**, 102002 (2006).
- [10] For a recent review, see N. Brambilla *et al.*, *Eur. Phys. J. C* **71**, 1534 (2011).
- [11] B. Aubert *et al.* (BABAR Collaboration), *Phys. Rev. Lett.* **95**, 142001 (2005); J. P. Lees *et al.* (BABAR Collaboration), *Phys. Rev. D* **86**, 051102(R) (2012); Z. Q. Liu *et al.* (Belle Collaboration), *Phys. Rev. Lett.* **110**, 252002 (2013).
- [12] B. Aubert *et al.* (BABAR Collaboration), *Phys. Rev. Lett.* **98**, 212001 (2007); X. L. Wang *et al.* (Belle Collaboration), *Phys. Rev. Lett.* **99**, 142002 (2007); B. Aubert *et al.* (BABAR Collaboration), arXiv:1211.6271.
- [13] J. Beringer *et al.* (Particle Data Group), *Phys. Rev. D* **86**, 010001 (2012).
- [14] M. Ablikim *et al.* (BESIII Collaboration), *Phys. Rev. Lett.* **110**, 252001 (2013).
- [15] Feng-Kun Guo, Christoph Hanhart, Ulf-G. Meissner, Qian Wang and Qiang Zhao, *Phys. Lett. B* **725**, 127 (2013).
- [16] M. Ablikim *et al.* (BESIII Collaboration), *Nucl. Instrum. Methods Phys. Res., Sect. A* **614**, 345 (2010).
- [17] M. Ablikim *et al.* (BESIII Collaboration), arXiv:1309.1896.
- [18] E. V. Abakumova, M. N. Achasov, V. E. Blinov, X. Cai, H. Y. Dong, C. D. Fu, F. A. Harris and V. V. Kaminsky *et al.*, *Nucl. Instrum. Meth. A* **659**, 21 (2011).

- [19] S. Jadach, B. F. L. Ward, and Z. Was, *Comput. Phys. Commun.* **130**, 260 (2000); *Phys. Rev. D* **63**, 113009 (2001).
- [20] P. Golonka, and Z. Was, *Eur. Phys. J. C* **45**, 97 (2006).
- [21] A. Ablikim *et al.* (BESIII Collaboration), *Phys. Rev. D* **86**, 071101(R) (2012).
- [22] X. L. Wang *et al.* (Belle Collaboration), *Phys. Rev. D* **87**, 051101(R) (2013).
- [23] E. A. Kuraev and V. S. Fadin, *Yad. Fiz.* **41**, 733 (1985) [*Sov. J. Nucl. Phys.* **41**, 466 (1985)].
- [24] Kuang-Ta Chao, Zhi-Guo He, Dan Li, Ce Meng, arXiv:1310.8597.
- [25] C. Z. Yuan (for the Belle Collaboration), arXiv:0910.3138 [hep-ex]. We take 5% from the range presented in the paper of $2.3\% < \mathcal{B}[X(3872) \rightarrow \pi^+\pi^-J/\psi] < 6.6\%$ at 90% C.L.